The Astronomical Journal, 135:1998–2012, 2008 June doi:10.1088/0004-6256/135/6/1998

THE NATURE AND ORIGIN OF SUBSTRUCTURE IN THE OUTSKIRTS OF M31. I. SURVEYING THE STELLAR CONTENT WITH THE *HUBBLE SPACE TELESCOPE* ADVANCED CAMERA FOR SURVEYS*

J. C. Richardson[1], A. M. N. Ferguson[1], R. A. Johnson[2], M. J. Irwin[3], N. R. Tanvir[4], D. C. Faria[3], R. A. Ibata[5], K. V. Johnston[6], G. F. Lewis[7], A. W. McConnachie[8], and S. C. Chapman[3]

[1] Institute for Astronomy, University of Edinburgh, Royal Observatory, Blackford Hill, Edinburgh EH9 3HJ, UK; jcr@roe.ac.uk
[2] Department of Astrophysics, University of Oxford, Keble Road, Oxford, OX1 3RH, UK
[3] Institute of Astronomy, University of Cambridge, Madingley Road, Cambridge, CB3 0HA, UK
[4] Department of Physics and Astronomy, University of Leicester, LE1 7RH, UK
[5] Observatoire de Strasbourg, 11, rue de l'Université, F-67000 Strasbourg, France
[6] Department of Astronomy, Columbia University, New York, NY 10027, USA
[7] Institute of Astronomy, School of Physics, A29, University of Sydney, NSW 2006, Australia
[8] Department of Physics and Astronomy, University of Victoria, Victoria, BC V8P 1A1, Canada
Received 2007 December 19; accepted 2008 March 16; published 2008 April 24

ABSTRACT

We present the largest and most detailed survey to date of the stellar populations in the outskirts of M31 based on the homogeneous analysis of 14 deep *Hubble Space Telescope* Advanced Camera for Surveys (*HST*/ACS) pointings spanning the range 11.5 kpc $\lesssim R_{\rm proj} \lesssim$ 45 kpc. Many of these pointings sample coherent substructure discovered in the course of the Isaac Newton Telescope Wide Field Camera (INT/WFC) imaging survey of M31 while others sample more diffuse structure in the extended disk. We conduct a quantitative comparison of the resolved stellar populations in these fields and identify several striking trends. The color–magnitude diagrams (CMDs), which reach $\gtrsim$3 mag below the red clump with high completeness, can be classified into two main categories based on their morphologies. "Stream-like" fields, so named for their similarity to the CMD of the giant stellar stream, are characterized by a red clump that slants blueward at fainter magnitudes and an extended horizontal branch. They show no evidence for young populations. On the other hand, "disk-like" fields exhibit rounder red clumps with significant luminosity width, lack an obvious horizontal branch, and show evidence for recent star formation (∼0.25–2 Gyr ago). We compare the spatial and line-of-sight distribution of stream-like fields with a recent simulation of the giant stream progenitor orbit and find an excellent agreement. These fields are found across much of the inner halo of M31, and attest to the high degree of pollution caused by this event. Disk-like material resides in the extended disk structure of M31 and is detected here up to $R_{\rm proj} \sim 44$ kpc; the uniform populations in these fields, including the ubiquitous presence of young populations, and the strong rotation reported elsewhere are most consistent with a scenario in which this structure has formed through heating and disruption of the existing thin disk, perhaps due to the impact of the giant stream progenitor. Our comparative analysis sheds new light on the likely composition of two of the ultra-deep pointings formerly presented as pure outer disk and pure halo in the literature.

Key words: galaxies: evolution – galaxies: formation – galaxies: halos – galaxies: individual (M31) – galaxies: stellar content – galaxies: structure

1. INTRODUCTION

A key goal of modern astrophysics is to understand the formation history of galaxies like our own Milky Way. The favored paradigm of hierarchical assembly within a cold dark matter (ΛCDM)-dominated universe predicts that spheroidal galaxy components form through a repetitive process of galaxy mergers and the accretion of smaller subsystems while disks arise from the smooth accretion of gas (e.g., White & Frenk 1991; Steinmetz & Navarro 2002). Recently, much ground has been gained in understanding the nature of stellar halos built up by tidal stripping of accreted sub-halos through N-body plus semi-analytical models (Bullock & Johnston 2005; Font et al. 2006a) and through numerical simulations (Helmi & White 1999).

Assuming that the accreted systems possess a stellar component, the most visible evidence of this hierarchical formation is expected in the form of tidal tails and partially digested satellites in the extended halos of galaxies (e.g., Bullock & Johnston 2005). Theoretical work on the tidal destruction of satellites by their massive hosts has shown that the mixing time of the debris depends on the satellites' mass and orbit. This timescale can be relatively short for debris in the inner galaxy but many gigayears for the outer galaxy (Johnston et al. 1996). Searches for spatially coherent tidal features in the extended halos of galaxies thus provide a means to probe ΛCDM predictions on scales of individual galaxies. Once tidal features are found, detailed follow-up studies of their stellar content and kinematics provide important constraints on the nature and number of objects which have merged. The Milky Way hosts at least one major tidal stream, originating from the Sagittarius dwarf (Majewski et al. 2003), with many others suggested (e.g., Grillmair & Dionatos 2006; Belokurov et al. 2007).

It can be argued, however, that the best current laboratory for studying faint stellar substructure around galaxies is provided by our nearest giant neighbor, M31. Our external view of this system removes complications due to line-of-sight and extinction/crowding effects that plague Milky Way studies, and, as a result, the structures observed in M31 are considerably easier to interpret. M31 has the been the subject of several deep wide-field ground-based surveys in the last decade and abundant low-surface brightness stellar substructure has been

* Based on observations made with the NASA/ESA *Hubble Space Telescope*, obtained at the Space Telescope Science Institute, which is operated by the Association of Universities for Research in Astronomy, Inc., under NASA contract NAS 5-26555.

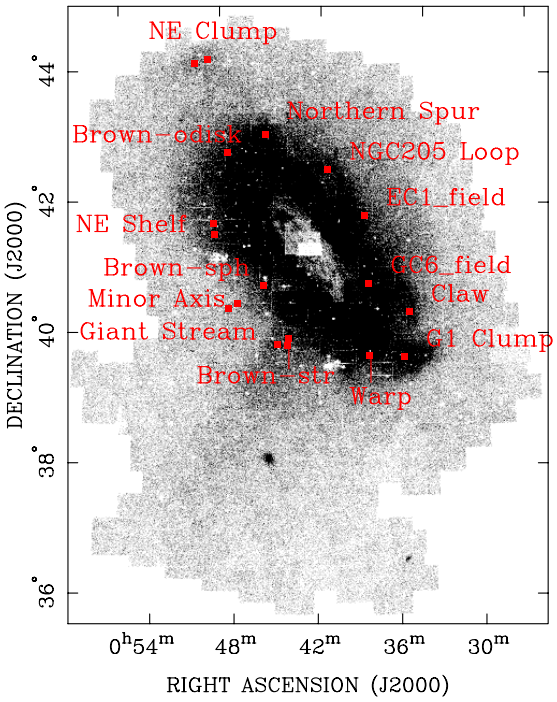

Figure 1. Map showing the distribution of RGB stars around M31 from the INT/WFC survey (Irwin et al. 2005). The image spans ∼95 kpc × 125 kpc. The locations of our *HST*/ACS pointings are overlaid in red, each covering 0.8 kpc × 0.8 kpc at the distance of M31.

found. These surveys have the depth to resolve individual red giant branch (RGB) stars in the halo of M31 and the analysis of their large-scale spatial density distribution has allowed unprecedented surface brightness levels to be reached ($\Sigma_V \gtrsim$ 30 mag per square arcsecond). The Isaac Newton Telescope Wide-Field Camera (INT/WFC) panoramic survey was the first of these surveys to be conducted and imaged the outer disk and inner halo of M31 out to a radius of ∼55 kpc, revealing copious substructure and tantalizing evidence for metallicity variations (Figure 1, see also Ibata et al. 2001; Ferguson et al. 2002; Irwin et al. 2005). In the southern quadrant, a giant stream (hereafter GS) was discovered falling into the center of M31 from behind (Ibata et al. 2001; McConnachie et al. 2003; Ibata et al. 2004). Prominent stellar overdensities were also discovered along both major axes, beyond the extent of the bright disk. More recently, the entire southern quadrant of M31 has been imaged out to a radius of ∼150 kpc, with an extension to the galaxy M33 at ∼200 kpc, using Megacam on the Canada–France–Hawaii Telescope (CFHT) (Martin et al. 2006; Ibata et al. 2007). This survey has revealed an additional complex system of even fainter tidal streams in the far outer halo, including a series of azimuthal streams along the minor axis out to ∼120 kpc. The Megacam survey has probed the GS out to a projected radius of ∼100 kpc, and uncovered evidence for internal stellar populations variations. Current simulations suggest it can be explained as the trailing debris arm of a disrupted dwarf galaxy of mass $\sim 10^9\ M_\odot$ whose leading arm may have wrapped around the inner galaxy at least twice (Mori & Rich 2008; Fardal et al. 2007, and references therein). The highly radial orbit of the stream suggests it passes very close to the center of M31 (Ibata et al. 2004), and hence almost certainly interacts with the disk. This may represent one of the most significant accretion events since the initial formation of M31, providing us with a fortuitous glimpse of ongoing mass assembly in the $z = 0$ universe. The presence of the GS has raised many questions: what role has this particular event played in the late formation history of M31? How much of the other inner halo debris has come from the stream? What damage has the stream progenitor done to the M31 disk? To what extent have other recent satellite accretions contributed to the growth of the halo?

As a means to address these questions, we have been using the Advanced Camera for Surveys (ACS) on board the *Hubble Space Telescope* (*HST*) to develop a better understanding of the origin and nature of the stellar substructure observed around M31. Ferguson et al. (2005) presented the first detailed color–magnitude diagrams (CMDs) of six regions of prominent inner halo substructure, reaching several magnitudes below the red clump (RC). Analysis revealed distinct variations in the stellar populations throughout many of the regions studied, consistent with the substructure having more than one origin. Two of the regions studied, the NE Shelf and the GS, were shown to have remarkably similar populations but different line-of-sight distances, consistent with the shelf being a forward wrap of the stream (Ferguson et al. 2005). A detailed examination of the stellar populations in one of the prominent major axis overdensities, the G1 Clump, was presented by Faria et al. (2007). This field, which lies at ∼30 kpc, was shown to have experienced continuous yet declining star formation during the last 10 Gyr and have a relatively high metallicity of $[M/H] = -0.4$ dex. Faria et al. (2007) argued that these properties are more consistent with those of the M31 outer disk than a low-mass accreted dwarf, and suggested that this piece of substructure could have been recently torn off from the main disk. Ibata et al. (2005) have studied the kinematics of many of these features, finding an overall pattern of significant rotation. They hypothesize that this extended and highly structured rotating structure has been formed by accretion.

In parallel to our efforts to understand the large-scale structure and stellar content of M31's outskirts, a number of ultra-deep pencil beam pointings have been obtained with *HST*/ACS (Brown et al. 2003, 2006a, 2006b, 2007). With upward of 32 orbits per pointing, these observations have been sufficiently deep to enable stars to be resolved to and below the oldest main-sequence turn-off, allowing the complete reconstruction of the star-formation history (SFH) in selected locations. Brown et al. (2006a) present results from inner halo fields they associate with the "tidal stream," "outer disk," and "spheroid." In all cases, the fields were shown to have experienced an extended SFH, and differences between them were quantified. Their spheroid field, which lies ∼11 kpc along the southern minor axis, was shown to be metal rich ($<[Fe/H]> \gtrsim -0.6$ dex) and with a substantial intermediate-age component. Interestingly, their tidal stream field, which lies very close to the GS field observed by Ferguson et al. (2005), showed almost identical populations (but being ∼1 Gyr younger). Finally, the outer disk field was best fit by populations of still higher metallicities and ages in the range 4–8 Gyr. The interpretation of these results has since been complicated by the suggestion that much of the inner halo, and in particular the southern minor axis, is "contaminated" by tidal debris torn off from the GS progenitor (e.g., Gilbert et al. 2007; Ibata et al. 2007). Indeed, in this paper we highlight the global extent of GS progenitor debris across the face of M31.

The halo of M31 is clearly highly complex, making it difficult to draw firm conclusions about the galaxy's assembly history from the study of only a few small fields. For example, it has recently been suggested that the studies claiming the stellar

Table 1
Observational Information

Field	Proposal ID	P.I.	R.A. (J2000)	Decl. (J2000)	Date	t_{F606W} (s)[a]	t_{F814W} (s)[b]
NGC205 loop	GO9458	A. Ferguson	00:41:11.6	42:29:43.1	2003-02-25	2475	5290
Minor axis	GO9458	A. Ferguson	00:48:08.4	40:25:30.0	2003-08-09	2400	5100
	GO9458	A. Ferguson	00:48:47.8	40:20:44.6	2003-08-04/05	2400	5100
NE shelf	GO9458	A. Ferguson	00:49:59.4	41:28:55.5	2003-07-31	2475	5290
	GO9458	A. Ferguson	00:50:05.7	41:39:21.4	2003-08-07	2400	5100
G stream	GO9458	A. Ferguson	00:44:15.5	39:53:30.0	2003-01-08	2430	5150
	GO9458	A. Ferguson	00:45:05.0	39:48:00.0	2002-10-17	2430	5150
N spur	GO9458	A. Ferguson	00:46:10.0	43:02:00.0	2003-07-08	2475	5290
G1 clump	GO9458	A. Ferguson	00:35:28.0	39:36:19.1	2003-01-17	2430	5150
Warp	GO9458	A. Ferguson	00:38:05.1	39:37:54.9	2003-06-10/11	2620	5240
Claw	GO10128	A. Ferguson	00:35:00.3	40:17:37.3	2005-01-06	2469	5210
NE clump	GO10128	A. Ferguson	00:51:56.7	44:06:38.5	2004-10-12	2469	5210
	GO10128	A. Ferguson	00:50:55.2	44:10:00.4	2004-10-09	2469	5210
EC1_field	GO10394	N. Tanvir	00:38:19.5	41:47:15.4	2005-07-10	1809	3000
GC6_field	GO10394	N. Tanvir	00:38:04.6	40:44:39.8	2005-07-23	1809	3000
Brown-stream	GO10265	T. Brown	00:44:18.0	39:47:36.0	2004-09-03/05	2460	5200
Brown-spheroid	GO9453	T. Brown	00:46:08.1	40:42:36.4	2002-12-02/03	2460	5200
Brown-odisk	GO10265	T. Brown	00:49:08.5	42:44:57.0	2004-12-20/22	2460	5200

Notes.
[a] Total exposure time in the F606W filter. Note that the warp and Brown fields analyzed here do not reach their full depths.
[b] Total exposure time in the F814W filter. Note that the Warp and Brown fields analyzed here do not reach their full depths.

halo of M31 is markedly different from that of the Milky Way may have drawn inaccurate conclusions due to comparing kinematically-selected Milky Way halo populations with highly polluted tracts of the M31 minor axis (Ibata et al. 2007; Gilbert et al. 2007). In this study, we have carried out a homogeneous analysis of 14 deep *HST*/ACS pointings, including the three Brown et al. (2006a) fields, which probe various regions in the inner halo ($R_{\rm proj} \lesssim 45$ kpc) and extended disk of M31. Many of these fields were specifically targeted as bright and/or unusual substructure identified in the course of the INT/WFC imaging survey, while others were taken from studies designed for other purposes. In this paper, we present a comparative analysis of these fields, and identify striking trends which indicate the inner halo is dominated by a complex mix of giant stream material and disrupted disk material. A future paper will present detailed SFH fits to these fields. In Section 2 we describe our observations. The photometric reduction and completeness testing are summarized in Sections 3 and 4. The analysis and results are presented in Section 5. Our interpretation of the results is discussed in Section 6 and summarized in Section 7.

2. OBSERVATIONS

The primary dataset analyzed here comes from our programs to obtain deep imagery of prominent substructure in the M31 halo (GO 9458 and GO 10128, PI Ferguson). Ten different regions in the M31 outskirts were targeted in the course of these studies and nine of these are presented in this paper (see Figure 1). Preliminary results on the stellar populations at six locations ("giant stream" (GS), "NE shelf," "minor axis," "NGC 205 loop," "northern spur," and "G1 clump") were previously presented in Ferguson et al. (2005). Each field was observed in the F606W (broad V) and F814W (broad I) filters with the Wide-Field Channel (WFC) of the ACS. Most of the fields were observed for one orbit in F606W and two orbits in F814W, resulting in accurate photometry to several magnitudes below the horizontal branch. The "warp" field was exposed for significantly longer; however, the analysis presented here is based on re-drizzled images to match the depth of the other fields. The minor axis, NE shelf, GS, and NE clump fields all consist of two separate pointings to increase star count statistics on otherwise low-density stellar fields.

We also utilize two fields ("EC1_field" and "GC6_field") which were observed as part of our imaging survey of newly discovered globular clusters in the outer M31 halo (GO 10394, PI N. Tanvir, see Mackey et al. 2006, 2007). These fields are somewhat shallower than the primary fields discussed above (one orbit in each of F606W and F814W), but they still provide good sensitivity to well below the horizontal branch. With the globular clusters masked out ($R \sim 30''$), the background field populations are very useful probes of diffuse structure in M31's extended disk. This is the first time results from the warp, NE clump, claw, EC1_field, and GC6_field have been published.

The remaining three fields in our study come from several of the ultra-deep programs of Brown (GO 9453 and GC 10265). These pointings are labeled "NGC224-Stream," "NGC224-Halo," and "NGC224-Disk" in the *HST* archive, though for clarity here we reassign the names "Brown-stream," "Brown-spheroid," and "Brown-odisk," respectively. For each field, we retrieved a set of exposures from the *HST* archive and drizzled them to an equivalent depth of our primary fields. The full-depth pointings have already been thoroughly explored and are the subject of several papers (Brown et al. 2003, 2006a, 2006b). We note that although the Brown-stream field is sandwiched between our own GS pointings, we have chosen to keep it separate rather than co-add it for comparative purposes. The complete observational information for each pointing analyzed here is given in Table 1.

3. DATA REDUCTION AND PHOTOMETRY

All of the fields were subject to the same method of reduction and analysis. Pipeline-calibrated images were retrieved from the

HST archive and, for each field, those images in a given filter were combined with the PyRAF TWEAKSHIFTS and MULTIDRIZZLE tasks (Koekemoer et al. 2006). TWEAKSHIFTS was first used to calculate any residual offsets between images after applying the WCS information from the input headers. Such shifts were generally found to be $\lesssim$0.5 pixel in the case of images taken within a given visit and $\lesssim$1 pixel for images taken across different visits. MULTIDRIZZLE was then invoked to register and stack images using these corrected shifts. The final drizzles were conducted using the Lanczos3 kernel with pixfrac and scale set to unity.

Before photometering the images, masks were constructed on the F814W frames to cover diffraction spikes, bright background galaxies, and saturated stars, and then applied to the F606W images. Photometry was performed on the co-added images using the stand-alone version of DAOPHOT-II (Stetson 1987). The stellar density in our fields was typically low to moderate. Tests revealed that tighter CMD sequences generally resulted from aperture photometry alone; however, full point-spread function (PSF) fitting photometry was also carried out as a means to discriminate between stars and galaxies (see also Ferguson et al. 2005; Faria et al. 2007). After a first pass of object detection and aperture photometry, ~250 candidate PSF stars were selected from the star catalogue on the basis of their isolation, brightness, and lack of obvious nearby artifacts. In creating an empirical PSF for each field in each pass band, any star whose fit was flagged as lying 1σ or more from the mean χ^2 value was removed from the PSF candidate star list and the PSF redefined. The initial guess (non-varying) PSF model was fit to all sources in the catalogue with ALLSTAR II.

Subsequently, all stars, except PSF candidate stars, were fit and subtracted from the image and an improved PSF model was built and then re-fit to the entire star catalogue. This process was iterated, allowing the PSF model to vary linearly with position across the frame, until the χ^2 statistic of PSF candidate star fits was minimized and the number of stars retained by ALLSTAR II had converged. A further pass of object detection and PSF-fitting photometry was carried out on a star-subtracted frame to reveal stars previously missed. Finally, the best-fit PSF model was fit to all stars in the catalogue. The photometry list was pruned by rejecting stars with any of χ^2, magnitude error or sharpness lying outside 3σ of the average value at that magnitude, yielding a final list of stellar sources for which we subsequently adopted their aperture photometry. The two catalogues (F814W and F606W) for each pointing were then matched to within two pixels. In total, approximately 675,000 stars were retained for analysis.

We then corrected the photometry for aperture effects. The 2–4 pixel (0.″05–0.″10) radii aperture corrections were calculated using the average value from the photometry of the pruned, matched list of PSF candidate stars. The 4 to "infinite" pixel aperture correction was taken from Sirianni et al. (2005). Magnitudes were placed on the VEGAmag system utilizing the zero-point values of Sirianni et al. (2005) and corrected for foreground reddening by interpolating within the maps of Schlegel et al. (1998) (see Table 2). The photometry has not been corrected for reddening internal to M31; however, this correction is not expected to be significant for most of our fields since they lie outside the main gas disk. Table 2 lists the reddening, internal HI column densities, projected and de-projected radial distances of each field, and is ordered according to increasing projected radial distance from the center of M31. We did not correct for charge transfer efficiency (CTE) because these data were obtained early in the lifetime of the ACS when the cumulative damage caused by radiation was minimal (see also Brown et al. 2006a). Hereafter, all magnitudes refer to de-reddened magnitudes in the VEGAmag system.

Table 2
Distance and Reddening

Field	$E(B-V)$[a]	N(H I)[b] (10^{19} cm^{-2})	$R_{\rm proj}$[c] (kpc)	$R_{\rm disk}$[d] (kpc)
Brown-spheroid	0.081	0.65	11.5	53.0
EC1_field	0.070	>0.10	13.2	60.5
GC6_field	0.074	11.0	13.8	26.1
NGC205 loop	0.076	...	17.0	71.5
Minor axis	0.060	0.64	17.9	91.8
	0.059	>0.10	19.9	82.7
NE shelf	0.065	>0.10	18.6	54.3
	0.071	>0.10	19.3	59.5
G stream	0.058	>0.10	19.0	79.5
	0.051	>0.10	20.7	68.4
Brown-stream	0.053	>0.10	20.3	72.7
Claw	0.060	1.20	23.7	42.0
Warp	0.054	9.80	25.1	31.1
N spur	0.079	0.10[e]	25.3	43.3
Brown-odisk	0.080	35.0[e]	25.6	25.6
G1 clump	0.063	26.0	29.2	29.7
NE clump	0.093	1.20[e]	44.1	59.0
	0.092	1.00[e]	44.6	53.0

Notes
[a] Values from the reddening map of Schlegel et al. (1998).
[b] M31 column densities; D. Thilker, private communication.
[c] Projected radial distance.
[d] De-projected radial distance calculated assuming an inclined disk with P.A. = 38.1° and i = 77.5°.
[e] Line-of-sight subject to MW confusion.

4. COMPLETENESS

The morphology of a CMD reflects the fraction of stars in different evolutionary phases; the precise location of a star within a given phase is a function of both age and metallicity. It is necessary to have a good understanding of how complete the CMD is as a function of magnitude and color before detailed interpretation. An artificial star test algorithm was employed to empirically calculate the photometric scatter and completeness of the data. Each image had several thousand artificial stars of a specific magnitude (spanning the range 30.0–20.0 mag in 0.5 mag steps) added randomly, where each artificial star is a scaled version of the best-fit PSF model. The aim is to add as many artificial stars as possible to gain sufficient statistics, but not so many as to significantly crowd the field. It was found that adding ~10% of the total number of real stars found per band satisfied this condition in all fields. The artificial stars are recovered, with no prior knowledge regarding their positions, using the identical method employed for the real data. They are pruned using the same parameters derived from pruning the original photometry, not least since the excess artificial stars at the magnitude being tested could skew the 3σ levels used in the pruning process. The resulting catalog is compared with the actual input positions of the artificial stars in order to derive the success rate of recovery. Steps are taken to avoid the accidental inclusion of real stars close to, or superimposed on, artificial star positions. Artificial stars coincident with a brighter real star are rejected, while artificial stars coincident with fainter real stars are retained but considered to have contaminated photometry.

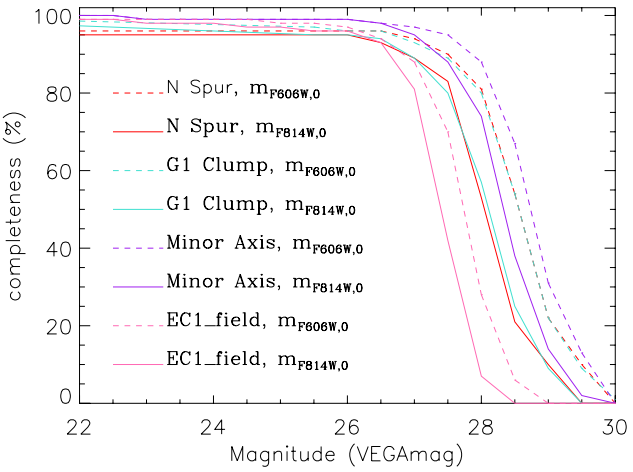

Figure 2. Results of the artificial star tests on representative fields of high, low, and intermediate stellar crowding as demonstrated by the variation in completeness as a function of magnitude for the spur, minor axis, and G1 clump, respectively. Also shown is the completeness function for the EC1 field which, along with GC6, has a reduced exposure time relative to the other fields analyzed here.

The process is repeated until the entire magnitude range has been covered.

Figure 2 shows the completeness rate as a function of magnitude for fields spanning a range of stellar densities, as well as for one of the shallower fields. For the bulk of our fields, completeness levels exceed 80% at $m_{F606W} = 28.0$ mag and $m_{F814W} = 27.5$ mag. For the slightly shallower EC1_field and GC6_field, these limits drop to 27.25 mag and 27.0 mag, respectively. Thus, a high completeness is maintained to generally $\gtrsim$2 mag below the RC. As expected, the higher-density fields have somewhat lower completeness at a given magnitude. Analysis of the photometric errors as a function of magnitude and color as derived from artificial star tests demonstrates that magnitudes are accurate to $\lesssim$0.10 mag at $m_{F814W} = 26.5$ mag.

5. ANALYSIS AND RESULTS

5.1. Color–Magnitude Diagrams

Figure 3 shows the CMDs of all of the fields represented as Hess diagrams with a square-root stretch. The total number of stars detected in each field is given below the name, and error bars are plotted as derived from artificial star tests. The ridge-line of 47 Tuc (NGC104: [Fe/H] = −0.7, 12.5 Gyr) as taken from Brown et al. (2005) is superimposed on the CMDs. It has been transferred into the VEGAmag photometric system using the appropriate zero-points from Sirianni et al. (2005), corrected to the M31 distance modulus of $(m - M) = 24.47$ (McConnachie et al. 2005), and de-reddened. The CMDs appear broadly similar; all have wide RGBs and prominent RCs typical of M31 populations seen at smaller radii (e.g., Mould & Kristian 1986; Holland et al. 1996; Ferguson & Johnson 2001; Bellazzini et al. 2003; Ferguson et al. 2005; Brown et al. 2006a). The RGB widths are considerably larger than the photometric error bars for magnitudes brighter than $m_{F814W} < 26$ mag suggesting an intrinsic spread in metallicity. The high proportion of RGB stars with colors redder than the 47 Tuc ridge-line suggests that these stellar populations extend to high metallicities ([Fe/H] $\gtrsim -0.7$ dex). The warp, GC6_field, and Brown-odisk fields reach further to the red than other fields. Since these fields are amongst those with the highest H I column densities (see Table 2), it is possible that internal extinction is also contributing to the color of the RGB. On closer inspection, several morphological differences are apparent between the CMDs in Figure 3. The most striking of these is the morphology of the RC and horizontal branch (HB) features produced by core Helium burning stars. In many of the CMDs, the RC slants blueward at fainter magnitudes (hereafter referred to as the blue RC[8]) and is accompanied by an extended horizontal branch. In contrast, many of the other CMDs show fairly round RCs which have a significant luminosity, but little color spread and no evidence for an extended horizontal branch. Additionally, these fields also show evidence for blue plumes (BPs) of upper main-sequence (i.e., young) stars. If extended blue HBs are also present in these fields, they would partly overlie the BPs making direct detection difficult. One further characteristic common to many of the latter set of fields is a prominent overdensity to the left of the RGB at $m_{F814W} \sim 26.1$ mag. This feature has the correct magnitude and color to be a main-sequence turn-off of a 2–3 Gyr population (Girardi et al. 2000). For reasons which will become apparent later on, we assign the terms "stream-like" and "disk-like," respectively, to these different CMD behaviors. Note that while CMDs within a given group share a strong morphological resemblance, they need not be composed of exactly identical populations. Indeed, the average best-fit age and metallicity of the Brown-stream and Brown-spheroid fields, both classified here as "stream-like," have been found to differ by 0.1 dex and 0.9 Gyr, respectively (Brown et al. 2006a).

Well-populated fields in both categories exhibit a prominent RGB bump located below the RC ($m_{F814W} \sim 24.6$ mag, $m_{F606W} - m_{F814W} \sim 0.8$ mag) implying a metal-rich population. These features are the result of stars zig-zagging past the same luminosity value when the H burning shell passes the chemical discontinuity left behind by the expanding convective envelope causing a temporary drop in nuclear efficiency. The RGB bump luminosity is expected to decrease with respect to the RC as the metallicity increases though it can be difficult to interpret in the case of composite stellar populations. The most populated fields (NE shelf, N spur GC6_field, and warp) also feature asymptotic giant branch (AGB) bumps at $m_{F814W} \sim 23.1$ mag, $m_{F606W} - m_{F814W} \sim 0.9$ mag. For fields with both RGB and AGB bumps, the fact that their luminosities straddle the RC luminosity supplies an additional clue regarding their ages and metallicities. According to the RC models of Alves & Sarajedini (1999), such behavior indicates that these populations are relatively metal rich. Further, for a single stellar population of [Fe/H] = −0.7 dex, this behavior implies an age of at least ∼5 Gyr; however, this restriction is relaxed for more metal-rich populations

A few fields exhibit CMDs which share characteristics of both stream-like and disk-like behavior. For example, the Brown-odisk field has a round RC typical of disk-like fields, yet it also shows evidence for a low-level blue RC and even an extended HB. Another field with some overlap between the two groups is the NGC205 loop. As noted in Ferguson et al. (2005), this field has a blue RC but it lacks the strong RGB and AGB bumps seen in other stream-like fields. This is not just a statistical effect related to the stellar density on the CMD because the RGB bump is noticeably stronger in the Brown-stream field

[9] Often referred to as a red horizontal branch in the literature.

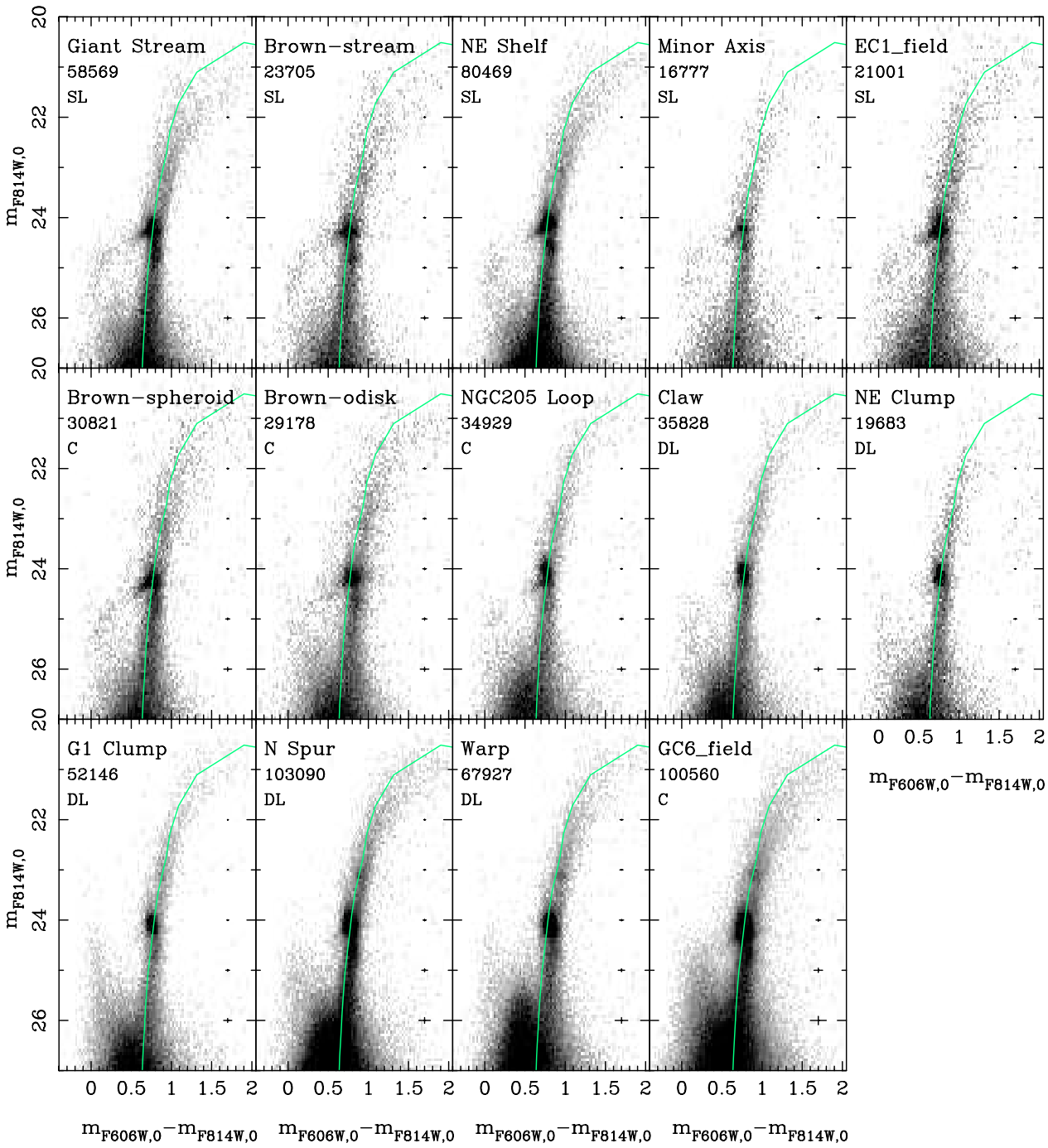

Figure 3. CMDs plotted as Hess diagrams with a square-root stretch to bring out fainter features such as RGB and AGB bumps. The bins are 0.025 mag in color and 0.062 mag in magnitude. The number of stars in each diagram is given below the name. The ridge line of 47 Tuc, which has [Fe/H] = −0.7 and age = 12.5 Gyr (Brown et al. 2005), has been shifted to the distance of M31 and overlaid. Photometric errors derived from artificial star tests are shown on the right-hand side of each CMD. The CMDs are $\gtrsim$90 % complete at $m_{F814W,0} = 27.0$ mag ($\sim$80% for EC1_field and GC6_field). Fields are labeled as disk-like (DL), stream-like (SL), or composite (C), as described in the text (Section 5.2).

which has ∼11,000 fewer stars. In addition, there is a hint of the bright main-sequence turn-off "hump" ubiquitous to our disk-like fields. In Figure 3, the Brown-spheroid appears very similar to the GS despite being originally presented as pure halo in the literature (Brown et al. 2003); this fact has also been noted by Brown et al. (2006a, 2006b). However, it will be shown in the following sections that there are important differences between these fields and that its true nature is likely a mixture of both GS and halo populations. These fields thus form a third category of "composite fields."

5.2. Differencing the Color–Magnitude Diagrams

Figure 4 shows the result of subtracting the normalized GS Hess diagram from the other fields, where the Hess diagrams have been normalized by the total number of stars with F814W

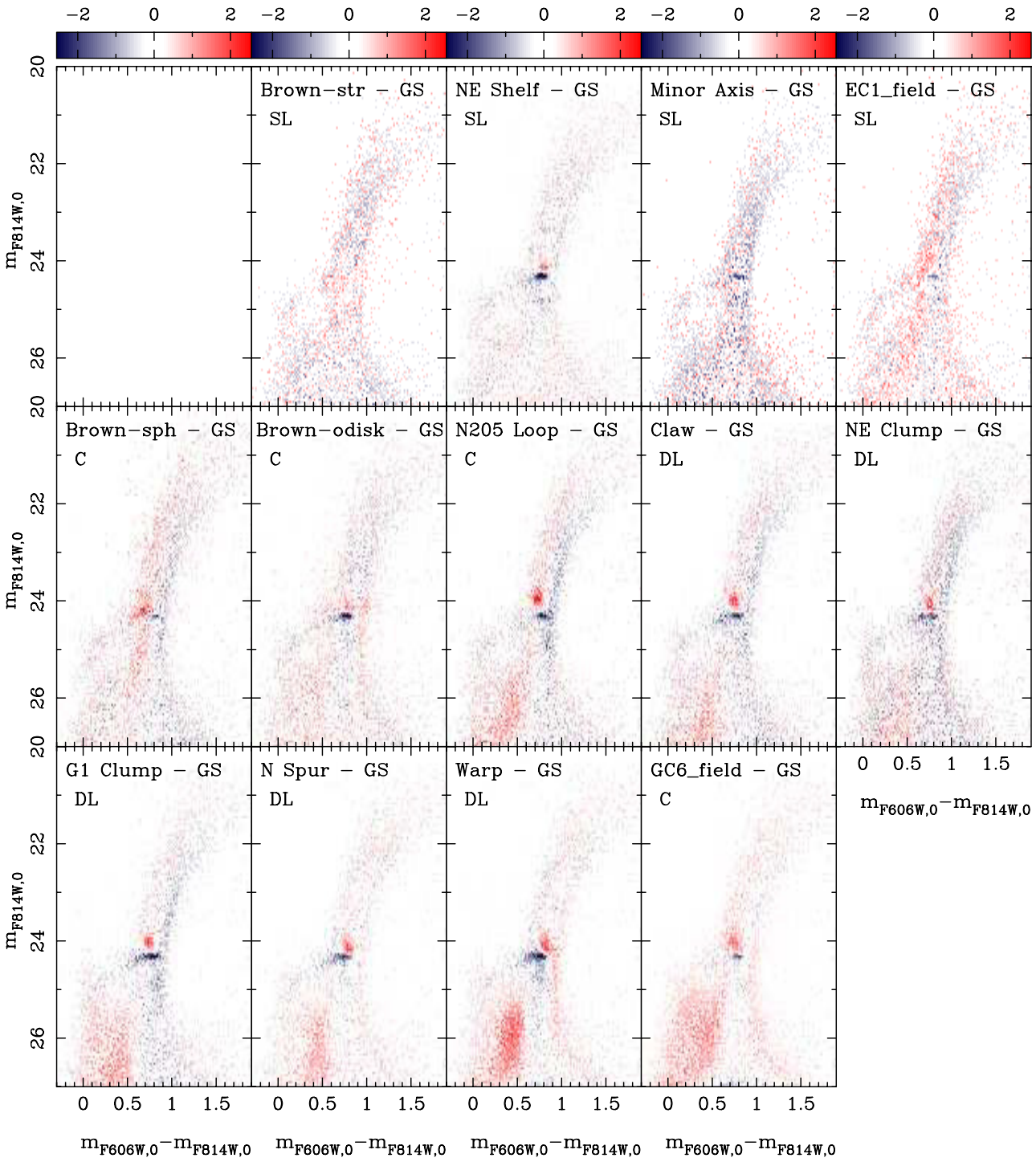

Figure 4. Comparisons of individual fields to the GS field. In each panel, the normalized Hess diagram of the field has been subtracted by the normalized GS Hess diagram to highlight the relative differences in the underlying populations. Red signifies an under-subtraction and blue an over-subtraction. The units are arbitrary and meaningful differences are strong, coherent overdensities in red or blue. Subtractions involving the minor axis, Brown-stream, EC1_field, and NE clump fields are noisy due to small number statistics.

band completeness over 90% ($m_{\rm F814W} < 27.0$ mag; corresponding to ∼80% in the shallower GC6_field and EC1_field). As expected, the stream-like fields show excellent agreement with the GS leaving negligible residual structure, except in the case of the NE shelf where the RC is brighter. Ferguson et al. (2005) have argued that this offset in RC magnitude is the effect of different line-of-sight distances; we will return to this point in Section 6.1. Using their ultra-deep CMD of the giant stream, Brown et al. (2006a) have derived an average age of 8.8 Gyr and average metallicity of [Fe/H] = −0.7 dex in their field. It

is, therefore, likely that this type of population dominates all the stream-like fields.

The subtractions reveal very clear differences between the disk-like fields compared to the GS, and simple line-of-sight distance shifts cannot bring the two into agreement. Disk-like fields display a significant over-subtraction of the blue RC (at $m_{F814W} \sim 24.3$ mag, $0.4 < m_{F606W} - m_{F814W} < 0.9$) and an equally prominent under-subtraction of the vertically elongated RC. In addition, they reveal varying degrees of under-subtraction of the blue main-sequence populations ($m_{F606W} - m_{F814W} \leqslant 0.6$ mag, $m_{F814W} \geqslant 25.5$ mag), indicating that these fields have much greater proportions of stars with younger ages than the GS. This residual young population is especially strong in the warp field. Several disk-like fields (the claw, NE clump, G1 clump, and N spur) also show a noticeable over-subtraction redward of their RGBs seen as a thin blue strip running parallel to the RGB for $m_{F814W} < 25.5$ mag suggesting that GS RGB stars extend to higher metallicities than these disk-like fields (note that this over-subtracted band is too wide to be caused by age differences alone).

The composite fields show differing patterns of residuals, none of which exactly mimic those seen in the disk-like fields. Despite the NGC205 loop CMD showing a blue RC, there is a strong over-subtraction of that feature in Figure 4, indicating that old metal-poor stars constitute a much smaller percentage of this population than in the GS. Indeed the subtraction has revealed that the NGC205 loop field has some disk-like properties: a RC elongated in luminosity, a "hump" consistent with bright main-sequence turn-off stars ($m_{F814W} \gtrsim 25.5$ mag, $m_{F606W} - m_{F814W} \lesssim 0.6$ mag), and an over-subtraction redward of the RGB. In terms of the subtracted Hess diagram, the NGC205 loop shows somewhat similar residuals to the disk-like claw field, although the under-subtracted RC is slightly bluer. The GS subtracts rather cleanly from the GC6_field although residuals confirm that it has an excess of younger and more metal-rich constituents. The Brown-odisk field exhibits smaller residuals in the region of the RC/HB than disk-like fields, implying the possibility of a stream-like contribution to the population in this region.

The last composite field, the Brown-spheroid, displays the most unique subtraction signature. Although parts of the CMD are well matched by the GS, the red side of the RGB is strongly over-subtracted, suggesting that this field does not contain such high metallicities. Furthermore, the pattern of RC residuals reveals an excess HB sequence not seen in the GS, or any other fields. In figures throughout the paper, we will refer to fields as being either DL (disk-like), SL (stream-like), or C (composite) based on the Hess diagram subtractions.

5.3. The Intermediate/Old Populations

The Hess diagram subtractions have confirmed that the dominant differences between stream-like and disk-like CMDs are those features which reflect the composition of the old and intermediate-age core Helium burning components. We proceed here to put these differences on a more quantitative ground. Figure 5 shows the m_{F814W} luminosity function (LF) and color distribution in the region of the RC for each field. The region selected for the color distribution plots was $23.5 < m_{F814W} < 24.75$ and $-0.5 < m_{F606W} - m_{F814W} < 1.2$ to avoid the inclusion of BP stars. The dashed line represents the Gaussian fits to these distributions, using the fitting function formalism of Paczynski & Stanek (1998). At $m_{F814W} \sim 24.0$ mag, the typical peak RC magnitude, the data are well above 90% complete and the photometric errors in magnitude ($\lesssim$0.02 mag) and color ($\lesssim$0.03 mag) are small.

The RC absolute magnitude and color are a function of the age and metallicity of a population. For a given metallicity, old stars form a fainter RC than young stars. The presence of a bright, elongated RC signifies a predominantly metal-rich intermediate-age/young population (Girardi & Salaris 2001). For a population of known age and metallicity, the RC magnitude also acts as a standard candle, a fact we will exploit in Section 6.1. Figure 5 further indicates that the disk-like fields generally have brighter and slightly more elongated RCs than the stream-like fields, suggesting that they contain younger stellar populations in addition to the intermediate/old RGB components. In the absence of distance effects, the brighter peak magnitude could be the result of a contribution from the more evolved counterparts of the blue plume, that is, stars with the same age and metallicity but slightly larger masses than the young main-sequence turn-off stars which causes them to evolve into RGB stars more rapidly. The color distributions of the RCs are very similar, regardless of grouping, though there is marginal evidence for stream-like fields having slightly broader color widths. The peak magnitude and color of the G1 Clump ($m_{F814W} = 24.12$ mag, $m_{F606W} - m_{F814W} = 0.75$ mag) measured here are in excellent agreement with Faria et al. (2007).

As a test of the robustness of our RC measurements, as well as our photometry in general, we measured the RC color and magnitude on each individual CMD in those fields where we obtained double pointings (the GS, NE shelf, NE clump, and minor axis). The peak RC magnitudes and colors for the two separate pointings, as well as for our GS field and Brown-stream, are generally in excellent agreement, differing by no more than $\pm$0.03 mag. This indicates that the RC can be used as a distance indicator to an accuracy of $\pm$11 kpc. An unusual result was recovered in the case of the minor axis. In that field, the peak RC magnitudes differed by a sizeable 0.10 mag in the two different pointings. If the populations in these two pointings are identical, this magnitude variation would signify a puzzling $\sim$38.5 kpc line-of-sight difference despite a mere $\sim$2 kpc projected distance between them. More likely, we suspect that we have serendipitously discovered some small-scale substructure in this region with intrinsically different populations. The very low stellar density in the individual fields (combined these fields have <17,000 stars) precludes a detailed assessment of the similarity of the two CMDs; however, no obvious differences are apparent. It is interesting, however, that the inner of the two pointings contains twice as many stars as the outer.

Figure 6 compares the completeness-corrected RGB luminosity functions of stream-like and disk-like fields over the full luminosity range. The "stream-like" curve includes the GS, Brown-stream, NE shelf, minor axis, and EC1_field, while the "disk-like" curve includes the claw, NE clump, G1 clump, N spur, and warp. Composite fields are omitted. Individual fields in each group have first been shifted so that their peak RC magnitude matches the average of that group before being co-added and the LFs have been normalized at $m_{F814W} = 23.4$ mag, a point mid-way between the RC and AGB bump. This plot further emphasizes the gross differences between the two populations, including the different RC morphologies, with the disk-like function peaking at brighter magnitudes. In addition, stream-like populations appear to have a higher proportion of RGB bump stars than disk-like populations although the AGB

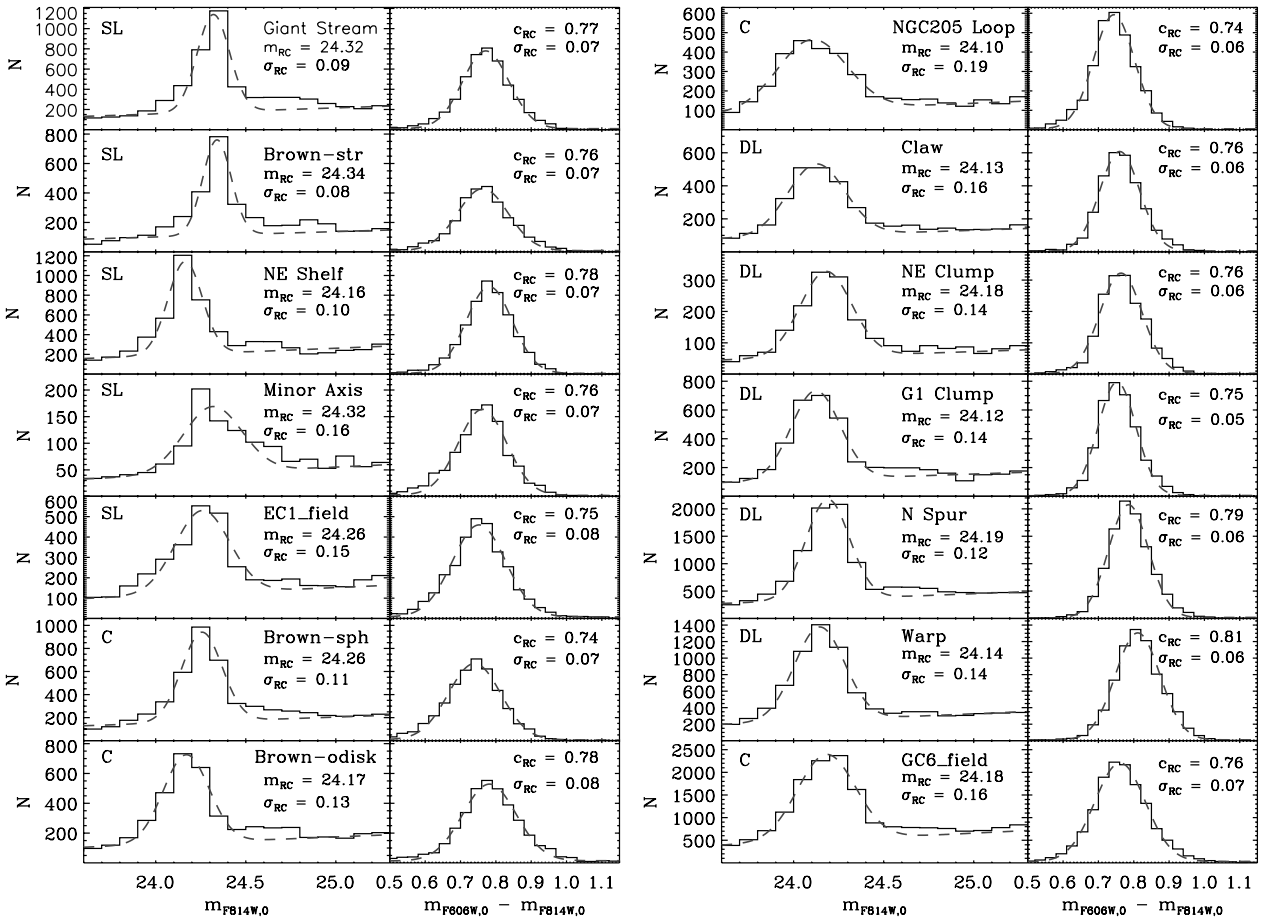

Figure 5. Gaussian fits (dashed line) to the red clump m_{F814W} luminosity function (left panels) and color distribution (right panels). m_{RC} refers to the peak m_{F814W} magnitude and c_{RC} to the peak $m_{F606W} - m_{F814W}$ color. Errors in the fits are ±0.01 in all cases except for the minor axis which has an error of ±0.02 in both m_{RC} and c_{RC}.

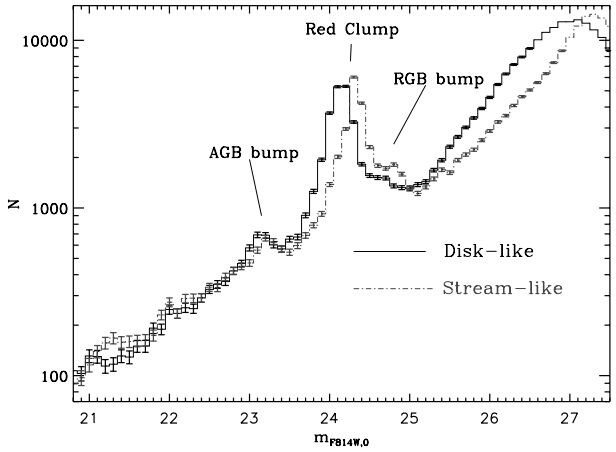

Figure 6. Comparing the completeness-corrected stream-like and disk-like RGB luminosity functions. The luminosity functions have been normalized at $m_{F814W} = 23.4$ mag, between the RC and AGB bump.

bumps are similarly concentrated. For magnitudes fainter than the RC, the disk-like LF rises more steeply than stream-like LF highlighting their young components as bright main-sequence turn-off stars merge into the RGB.

5.4. The Young Populations

Figure 3 indicates that the disk-like fields, and several of the composite fields have sub-populations of young stars. Full CMD-fitting is required to place rigorous constraints on the recent SFH of these fields, but we gain some quantitative insight by comparing their BPs with theoretical isochrones in Figure 7. The Girardi et al. (2000) isochrones of [Fe/H] = −0.4 dex with ages of 230 Myr, 630 Myr, 1.0 Gyr, 1.6 Gyr, and 2.0 Gyr best match the BP magnitude and color distribution. Lower-metallicity isochrones are too blue to match the BP, while more metal-rich isochrones are generally too red except in the cases of the GC6_field and warp where there is some overlap. Several fields show BPs which reach $m_{F606W} \sim 23$–24 mag, indicative of stars as young as a couple of hundred megayears old. It is particularly remarkable that such a young population is seen in the NE Clump, a field which sits at ∼44 kpc (or $R_{disk} \sim 56$ kpc).

In field populations, blue stragglers are thought to form by mass transfer between primordial binaries (Davies et al. 2004). These old blue straggler stars can masquerade as young main-sequence stars on a CMD (Carney et al. 2005) so it is important to address whether the BPs we see could be caused by such stars instead. Faria et al. (2007) provide a thorough discussion of this issue for the specific case of the G1 clump, and find that while this scenario cannot be completely ruled out, it is

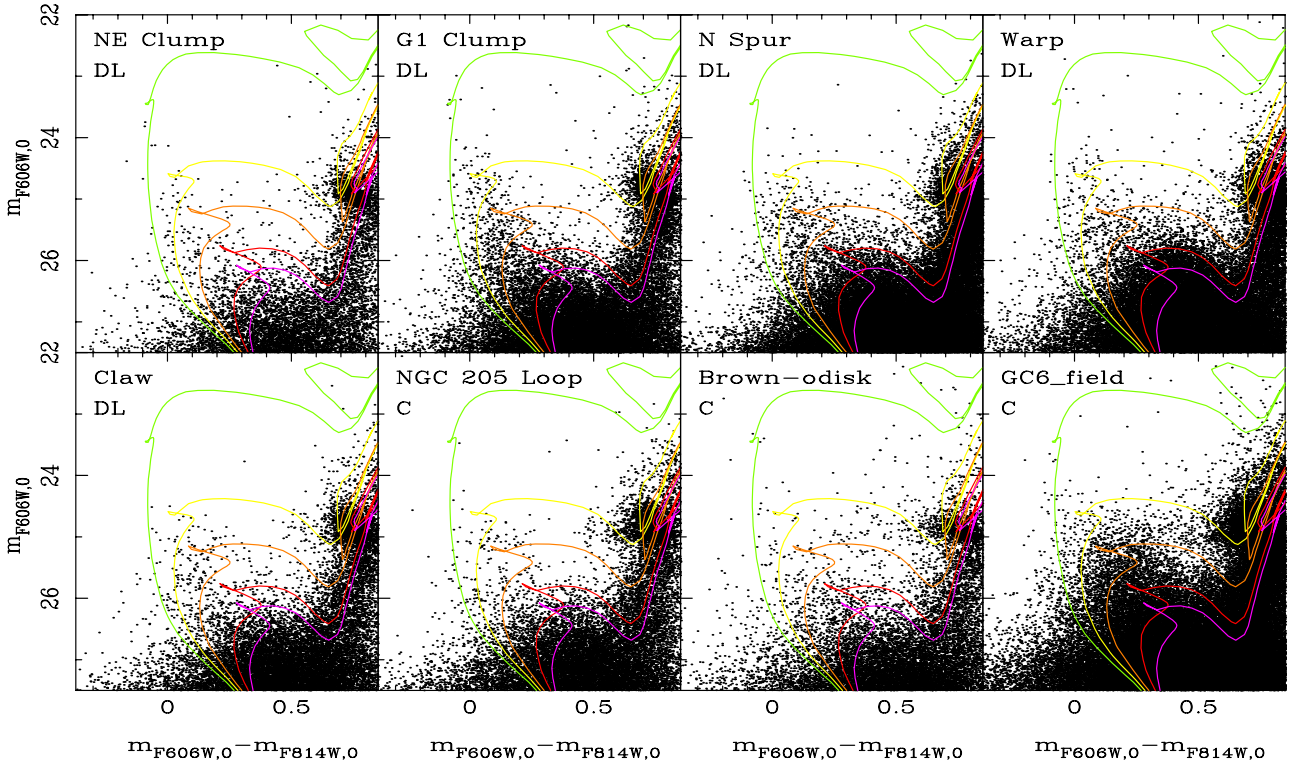

Figure 7. Close-up view of those fields containing blue plume populations. Isochrones from the Girardi et al. (2000) library of metallicity [Fe/H] = −0.4 dex and ages 230 Myr (green), 630 Myr (yellow), 1.0 Gyr (orange), 1.6 Gyr (red), and 2.0 Gyr (magenta) are overplotted. The density of stars falling between adjacent isochrones gives an estimate of the relative strength of star formation in that age bracket.

highly unlikely; these same arguments apply to all the fields presented here. If the BPs in our CMDs were made entirely of blue stragglers, the naive expectation would be that denser fields would have correspondingly dense BPs which is not observed. We also note that disk-like fields consistently have higher H I column densities than stream-like fields, further supporting the presence of genuinely young stars in these regions.

6. DISCUSSION

6.1. The Nature of the Stream-Like Fields

The discovery of the giant stream (Ibata et al. 2001) was the first spectacular indication that M31 is still accreting mass. Fields in our study which directly probe this substructure are the GS and Brown-stream fields, both lying at ∼20 kpc projected radial distance from M31 (see Figure 1). In addition, we have shown that the NE shelf, EC1_field, and minor axis fields have CMDs which are strikingly similar to the GS fields, indicating that these fields are also dominated by tidal debris stripped from the GS progenitor. Although these fields generally have smaller projected radii than disk-like fields, their positions correspond to larger distances in the plane of the disk.

Fardal et al. (2007) (hereafter F07) have recently presented an N-body simulation of the accretion of a dwarf satellite of mass $\sim 10^9\ M_\odot$ within a realistic M31 potential. Their simulation has been tailored to reproduce the GS and NE shelf as observed in Figure 1. As the satellite falls toward the galaxy, long tidal streams are produced, both leading and trailing the progenitor core. They identify the trailing stream as the giant stream, and suggest that the leading stream may have wrapped around the inner galaxy at least twice. Figure 8 shows the predicted distribution of the GS progenitor debris in their model with our *HST*/ACS pointings overlaid. Note that only satellite particles are represented; inside the black ellipse (which indicates the extent of M31's bright disk) a significant contribution of M31 disk stars is expected. As can be seen, there is an excellent overall agreement between the stream-like fields identified in this paper and the predicted pattern of debris. In particular, this includes the "western shelf" overdensity which is probed for the first time by our EC1_field. Figure 8 also indicates that much of the minor axis of M31 should be contaminated by diffuse GS debris stripped off during various pericentric passages (see Gilbert et al. 2007), and agrees with our finding that both the minor axis and Brown-spheroid fields have significant stream-like components. It is also encouraging that our disk-like fields, with the exception of the claw field which projects on the very edge of Fardal's western shelf, are found to lie well away from regions that contain stream debris in the simulation.

The three-dimensional distribution of stream debris is of great importance for placing constraints on the progenitor orbit (e.g., McConnachie et al. 2003). Ferguson et al. (2005) and Brown et al. (2006b) have exploited the similarity of the populations in stream-like fields to determine differential distances based on RC magnitudes. In particular, Ferguson et al. (2005) applied this to the GS and NE shelf fields, and derived that the latter lay closer to us than the former by a factor of 1.07 ± 0.01. The observed RC magnitude is distance dependent, so if we assume that the underlying populations in stream-like fields are the same, we can examine their differential line-of-sight distances by comparing their peak RC magnitudes. Table 3 presents a summary of the distance measurements to stream-like fields identified here. The observed distances have been determined by assuming that

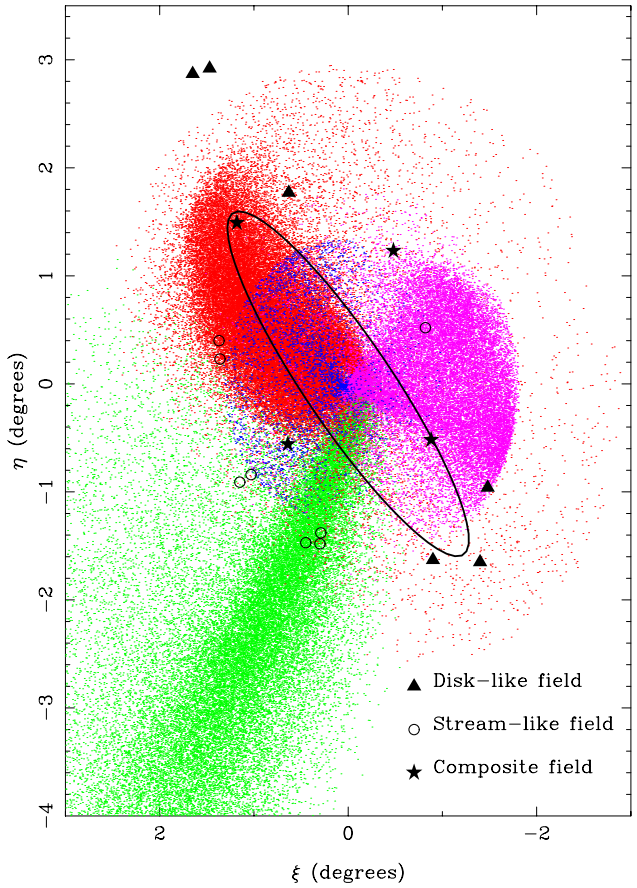

Figure 8. Locations of our fields with respect to the Fardal et al. (2007) simulation showing the predicted distribution of GS progenitor tidal debris around M31. Color coding is as follows: green particles represent the GS falling into its first pericentric passage; red particles show the fanning out of material into the north-east shelf after the first close pass and approaching their second pericentric passage; magenta particles show the fanning out of material into the western shelf after the second close pass and approaching their third pericentric passage and blue particles are heading for their forth pericentric pass. The locations of our 14 *HST*/ACS fields are overlaid (see Figure 1 for labels). The ellipse shows the approximate extent of M31's bright disk (R = 27 kpc, P.A. = 38.1° and i = 77.5°). The overlap between stream-like fields (open circles) and predicted coverage of stream debris is striking. Disk-like fields are represented by filled triangles and composite fields by filled stars.

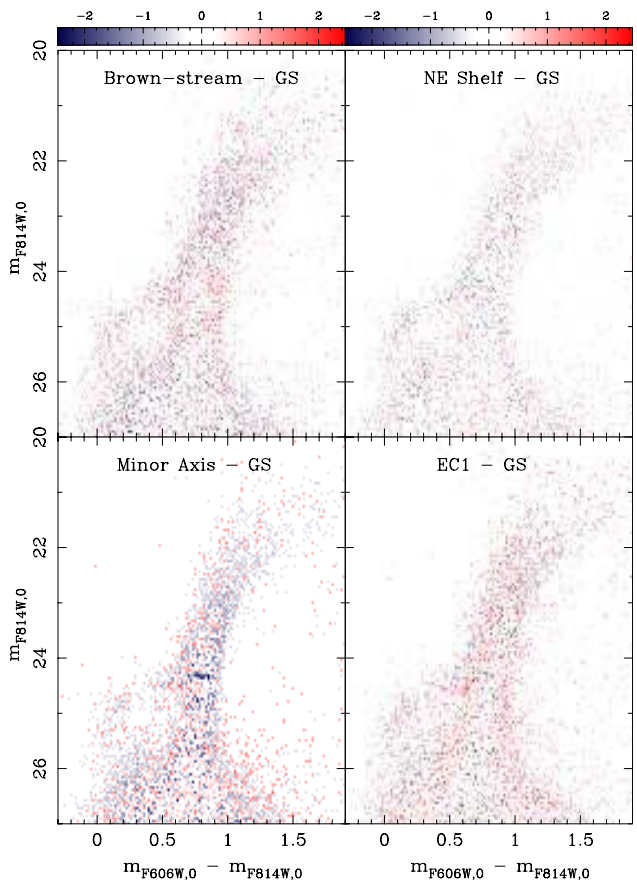

Figure 9. Same as Figure 4, but with stream-like fields shifted to the same line-of-sight distance as the GS field using RC color and magnitude information.

Table 3
Line-of-Sight Distances to Stream-like Fields

Field	D_{los}^{obs} [a] ±20 kpc	D_{los}^{sim} [a]	$F_{GS/field}^{obs}$ [b] ±0.03	$F_{GS/field}^{sim}$ [b]
Giant stream	830	816	...	...
EC1_field	807	795	1.03	1.03
Minor axis	785	785	1.06	1.04
NE shelf	769	745	1.08	1.10

Notes.
[a] Observed and simulated D_{los} calculated assuming M31 lies at D_{los} = 785 ± 25 kpc (McConnachie et al. 2005).
[b] Factor, $F_{GS/field}$, by which the GS lies further away from us than the field in question.

the GS field lies at D_{los} = 830 ± 20 kpc (Ferguson et al. 2005) with respect to M31 (D_{los} = 785 ± 25 kpc; McConnachie et al. 2005). The RC magnitude differences between the GS and other fields then yield relative distances from the center of M31. The line-of-sight depth of simulated particles is taken from Figure 2(b) of F07, set on an absolute scale using the same $D_{los}(M31)$. There is an excellent agreement in both the differential and absolute line-of-sight distances.

In using RC brightnesses to calculate approximate line-of-sight differences, we have implicitly assumed that all the stream-like fields have very similar underlying populations. To test the accuracy of this assumption, we have used the mean magnitude and color of the RC to shift all of the stream-like fields to the same line-of-sight distance and reddening as the GS field and then re-subtracted the GS Hess diagram (see Figure 9). These subtractions are much cleaner than those in Figure 4 and the residuals are consistent with Poisson noise. This lends support to the idea that they are composed of the same mix of stellar populations as the GS field. The minor axis retains a slight over-subtraction in the RC area, but it is unclear how significant this is given the sparsity of this field. Moreover, as we saw in Section 5.3, there may be small-scale population variations within this field.

6.2. The Nature of the Disk-Like Fields

Aside from sharing a common RC morphology, the disk-like fields are also distinguished by the presence of a young (⩽2 Gyr) population, the prominence of which varies from field to field. The NE clump, G1 clump, spur, GC6_field, and warp appear to have formed stars as recently as a few hundred megayears ago. There is no clear correlation apparent between

the strength of the BP population and either the projected or deprojected radial distance of the field, perhaps unsurprising given that the gas disk in M31 is known to be non-planar at large radius (Brinks & Burton 1984). However, there is a clear correlation between the presence of BP stars and the local H I column. For example, the fields with the highest unconfused H I column densities are the warp ($N_{\rm H\,I} = 9.8 \times 10^{19}\,{\rm cm}^{-2}$) and the G1 clump ($N_{\rm H\,I} = 26.0 \times 10^{19}\,{\rm cm}^{-2}$) which also exhibit the strongest BPs. This could suggest that the young stars seen have formed *in situ*.

It should be noted that disk-like fields are roughly aligned with the major axis and many (G1 clump, N spur, warp, claw, and the NE clump, in addition to the NGC205 loop) probe well-defined high surface brightness substructure lying within the extended disk of Ibata et al. (2005). This intriguing structure is characterized by strong rotation in the distance range $15\,{\rm kpc} \leqslant R \leqslant 40\,{\rm kpc}$, slightly lagging the thin disk component by $\sim$40 km s^{-1}, and has a modest velocity dispersion of 30 km s^{-1}. Ibata et al. (2005) have discussed various scenarios for the formation of the extended disk, and concluded the most likely one is via accretion. We revisit this important question here in light of the new stellar populations constraints we have derived.

6.2.1. Could Disk-Like Material Originate from One or More Accreted Satellite Galaxies?

The idea that the disk-like material results from the recent accretion of many small satellites provides a ready explanation for the jumbled morphology of the substructure. However, the homogeneity of the populations in the various fields—which are widely separated in distance in some cases—is problematic. Within the Local Group low-mass satellite galaxies generally obey a mass–metallicity relation and exhibit a range of star-formation and chemical-evolution histories (e.g., Dolphin et al. 2005). Models which explicitly take this into account predict that stellar halos should possess significant age and metallicity inhomogeneities resulting from accretion events with a range of satellite masses (Font et al. 2006a, 2007). As we have discussed, such differences are not observed in the disk-like substructure. Moreover, Font et al. (2007) have shown that young populations are not expected in tidal debris lying within the inner (<50 kpc) regions of hierarchically built halos.

An alternative scenario is one in which the disk-like material comes from a single accretion event involving a more massive satellite. Peñarrubia et al. (2006) have shown that an extended exponential disk structure can result from the accretion of a 10^9–$10^{10}\,M_\odot$ object on a coplanar prograde object. However, in order to reproduce the high degree of rotation observed in M31's extended disk, they require the progenitor to start on a circular orbit which is rather atypical for satellites observed in cosmological simulations (van den Bosch et al. 1999). Although the homogeneity of the underlying stellar population is not a problem in this scenario, the presence of genuinely young stars is rather puzzling. Indeed, this would seem to require that the disrupting satellite retains a substantial reservoir of gas until well within the potential of M31, even while much of its stellar component has already been stripped.

Could the source of disk-like substructure be the GS progenitor itself? As shown in Table 2, disk-like fields have H I column densities at least an order of magnitude larger than stream-like fields. It could be that the young populations in these fields have formed *in situ* and are unrelated to the dominant stellar component which has come from the stream. Our results discount this possibility. We have shown that the old and intermediate-age stars in stream-like fields have age and metallicity distributions which cannot be reconciled with those in disk-like fields, as reflected by their differing RC and HB morphologies. Furthermore, stream-like fields appear to have been more chemically enriched than disk-like fields at least a few gigayears before the present time. Current models predict "first contact" between the GS progenitor and M31 around $\sim$1 Gyr ago (e.g., Ibata et al. 2004; Fardal et al. 2006; Font et al. 2006b), so any material accreted onto the extended rotating disk would already have been more enriched than disk-like fields.

6.2.2. Could Disk-Like Material Originate from the Thin Disk?

The previous scenarios addressing the origin of disk-like material center upon idea that this material has been brought into M31 from another system. However, the presence of young stars in many extended disk fields begs the question as to whether this material could instead have formed in the gas-rich thin disk of M31, and subsequently been torn off and kicked out.

The G1 clump is the only disk-like field to have stringent constraints placed on its SFH so far. Faria et al. (2007) used STARFISH modeling (Harris & Zaritsky 2001) of the CMD to infer a high mean metallicity ([Fe/H] $= -0.4$ dex) and a large age spread ($\sim$10 Gyr). Although the bulk population is of intermediate-to-old age ($\gtrsim$6 Gyr), roughly 10% of its stellar mass has formed within the last 2 Gyr. As discussed by Faria et al. (2007), these properties are entirely consistent with those of the outer disk of M31 where trace amounts of recent star formation are commonly observed (Bellazzini et al. 2003; Williams 2001). In conjunction with its kinematic signature of disk-like rotation (Reitzel et al. 2004; Ibata et al. 2005), Faria et al. (2007) have suggested a connection between the thin disk and the G1 clump. In addition, Zucker et al. (2004) have suggested a link between the thin disk and the NE clump as one possible explanation of their observations. In view of the results presented here, we explore whether this interpretation can be extended to all of our disk-like fields.

If the disk-like material did originate in the thin disk, we require some mechanism capable of restructuring it and moving material out to large radii ($\sim$44 kpc in the case of the NE clump) and scale heights. Recent work has elucidated how interactions with sub-halos might heat, thicken, and perturb stellar disks, providing a method capable of producing such low-latitude substructure (e.g., Quinn et al. 1993; Walker et al. 1996; Velazquez & White 1999; Gauthier et al. 2006; Kazantzidis et al. 2007). Most recently, Kazantzidis et al. (2007) have performed hybrid cosmological plus numerical simulations of dark matter sub-halos bombarding a MW-type disk galaxy over an 8 Gyr period, and trace the impact on the host galaxy. They cull sub-halo properties such as mass functions and orbital parameters directly from cosmological simulations so that sub-halos are representative of their epoch. The cumulative effect of six such bombardments, one 60% as massive as the host's disk, is to produce several long-lived phenomena in the disk such as a significant flare, central bar, and coherent substructures akin to tidal streams. Most damage to the thin disk is caused by the most massive satellite. Significantly, although the thin disk is thickened and perturbed by these tidal interactions, forming many messy morphological features comparable to those observed in M31 and the MW, it survives intact to $z = 0$. Kazantzidis et al. (2007) only track the stellar particles in the original thin disk and not those of the interacting satellites. In reality, the content of the resultant disk will be a complex

mix of stars formed *in situ* as well as stars brought in by the satellite. While more work is required to establish the viability of this explanation, disk heating seems to explain many of the observed properties of disk-like fields (and the extended disk in general) at least on a qualitative level.

Many questions arise from this line of thought: will these discrete substructures ultimately disperse to form a thick disk in M31? Could the bulk of the damage to M31's disk have been caused by the impact of the GS progenitor? It is interesting to note that current simulations suggest the interaction between the GS progenitor and M31 began as recently as ∼1 Gyr ago (F07). This timescale agrees well with the dissolution timescale of discrete substructures in the extended disk, as estimated by Ibata et al. (2005). However, there are also suggestions that the GS was accreted 6–7 Gyr ago coinciding with the apparent cessation of star formation (Brown et al. 2006a). Font et al. (2007) present a comprehensive discussion of these two competing scenarios based on the results of their numerical simulations. The best estimates of the mass of the GS progenitor ($10^9\,M_\odot$) place it at the low end of the sub-halo mass range featured in Kazantzidis et al. (2007), yet it does have a highly radial orbit which was found to enhance the disruption to the thin disk. The simulation explained in Kazantzidis et al. (2007) resulted in a final distribution of disk stars best described by a thin + thick disk decomposition. There is room for much speculation, but we are unable to draw conclusions about this within the scope of this study.

6.3. The Nature of the Composite Fields

Our analysis has revealed that four fields—the Brown-odisk, GC6_field, NGC205 loop, and Brown-spheroid—do not fit neatly into either stream-like or disk-like categories. Several show traits from both. Can these populations be described as a simple combination of disk-like and stream-like material, or are they genuinely unique populations?

6.3.1. The GC6_field and Brown-odisk Fields

The CMDs of the Brown-odisk and GC6_field exhibit many disk-like properties, including prominent round RCs and BPs, reflecting their location at the edge of the main M31 disk ($R_{\rm disk}$ = 25.7 kpc and 26.8 kpc, respectively). However, these same fields also show evidence of an extended HB akin to that seen in stream-like fields. Furthermore, differencing their CMDs with the GS results in lower amplitude over-subtractions than found in disk-like fields (see Figure 4), implying a minority stream-like component to the stellar populations in these regions. If correct, this would be consistent with Figure 8 which indicates that both stream debris and thin-disk stars are expected in considerable proportions at these locations.

In order to test this further, a composite model CMD has been constructed using the N spur and GS fields and compared to the data in Figure 10. The ratio of disk to stream in the model has been scaled by eye to produce the cleanest subtraction. Overall, the residuals from this subtraction are of significantly lower amplitude than those in Figure 4, implying that this combination of fields is closer in nature to Brown-odisk and the GC6_field than the GS alone. In truth, these models are crude, but they serve to illustrate that these fields are likely disk-like fields contaminated by debris from GS. A more accurate breakdown of their populations will be achieved via full fitting of the star-formation histories in future work.

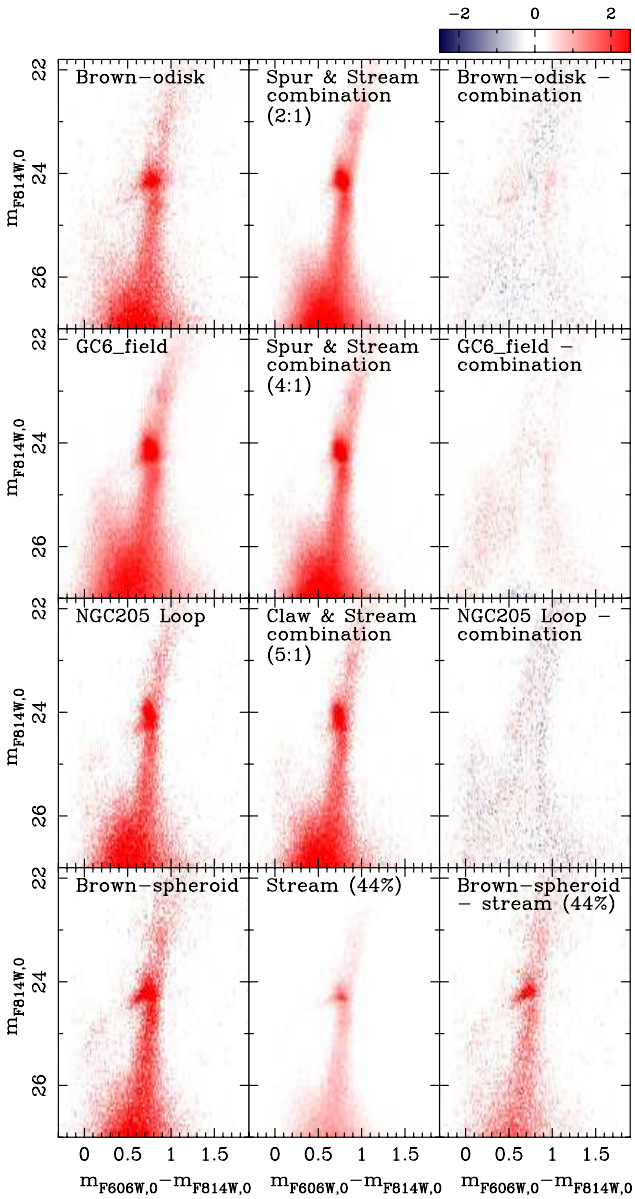

Figure 10. Examining the relative contribution of disk and stream material to the composite fields. The left-hand panels show the normalized CMDs of the composite fields while the middle panels show model CMDs created from differing amounts of the spur (or claw) and GS fields. The right-hand panels show the result of subtracting these models from the original Hess diagrams. As before, blue corresponds to an over-subtraction and red to an under-subtraction.

6.3.2. The NGC205 Loop Field

The NGC205 loop was so named because, on projected surface density maps, it appears as a tidal loop emanating from the dE NGC205 galaxy, which sits a mere ∼15 kpc away. Surface brightness profiles of NGC205 have long showed significant isophotal twisting implying tidal stripping of its material by M31 (Hodge 1973; Choi et al. 2002). Kinematics of stars thought to be associated with the NGC205 loop were presented by McConnachie et al. (2004), who identified two kinematic signatures, a majority component attributable to the M31 disk, and a small additional kinematically cold component ($\sigma_v \sim 10\,{\rm km\,s^{-1}}$) that they associate with the NGC205 loop. Subsequent examination of the same field by Ibata et al. (2005)

yielded no evidence for such bimodality, however, and led them to the conclusion that the NGC205 loop was part of the same vast extended rotating disk to which the disk-like fields belong (with $v_{\rm lag} \sim 14\,{\rm km\,s^{-1}}$, $\sigma_v \sim 36\,{\rm km\,s^{-1}}$).

We now turn to address what can be learnt about the origin of the NGC205 loop from its stellar populations. The NGC205 loop, despite its stream-like CMD, shows significant residuals in the GS subtraction which indicate a second stellar component is present at this location (Figure 4). Is this additional component tidal debris from NGC205 dwarf? Butler & Martínez-Delgado (2005) have recently examined the stellar populations in the outskirts of NGC205 and find a population characterized by a broad RGB, prominent RC and weak HB. They estimate a median metallicity of [Fe/H] > -1.06. The NGC205 loop residuals could be consistent with such a population. Indeed, the under-subtracted RC in this field is slightly bluer than that seen in the disk-like fields, suggesting that the excess population is more metal poor than the extended disk. On the other hand, a composite model made from the claw and the GS (5:1) produces a very good match to the CMD of the NGC205 loop in Figure 10. The apparent similarity of the intrinsic NGC205 dwarf stellar population to that of the extended disk makes it difficult to draw firm conclusions about the origin of the NGC205 loop. Better kinematical constraints and more detailed modeling of NGC205's orbital trajectory are required.

6.3.3. The Brown-Spheroid Field—a Glimpse of M31's Underlying Halo?

The Brown-spheroid field is unlike any of the other fields presented here. Although the GS subtraction is fairly clean, it has unveiled an excess extended blue HB population not seen in any other subtraction. This suggests the presence of a higher fraction of metal-poor and/or ancient stars than in the GS material. At $R_{\rm proj} = 11.5$ kpc, this is the innermost of our ACS pointings; if a weak smooth halo component exists in M31, then it is in this field that we would expect the strongest signature.

Gilbert et al. (2007) have recently revisited the nature of the Brown-spheroid field in light of their spectroscopic study of stars along the minor axis of M31. Based on kinematics, they estimate that ∼45% of stars in this field belong to a cold component. If we assume this component consists of debris from the GS progenitor we can take our analysis further. Figure 10 shows the result of subtracting a 44% GS component from the Brown-spheroid field. The residual population is characterized by an RC which has narrowed somewhat in luminosity, the lack of an RGB bump, and the presence of a prominent blue HB. It is tempting to speculate that this represents the true underlying halo of M31.

Our own minor axis field, which sits ∼8 kpc further out than the Brown-spheroid field, was originally intended to probe the uncontaminated halo; however, we have found here that it too shows the signature of contamination by stream debris. Gilbert et al. (2007) trace the kinematics in a location close to our minor axis field, finding that ∼31% of the stars are part of a cold giant stream-like component. It may appear surprising that this field compares so much better to the GS than the Brown-spheroid when the fraction of stream present is estimated to be even lower. However, it should be noted that the minor axis field lies at a very similar projected radial distance from the center of M31 as the GS field (see Table 2). Therefore, if the underlying M31 halo is spherical, the fraction of ancient metal-poor components in these two fields should be almost identical and thus cancel out cleanly in subtractions between the two.

7. SUMMARY

We have presented the largest and most detailed survey to date of stellar populations in the outskirts of M31. We have carried out a homogeneous analysis of 14 deep *HST*/ACS pointings spanning the range 11.5 kpc $\lesssim R_{\rm proj} \lesssim$ 45 kpc. These pointings sample well-defined substructure identified in the course of the INT/WFC imaging survey, as well as the more diffuse extended disk. We have shown how stellar populations in these fields can be generally divided into two clearly distinct categories based on their CMD morphologies: stream-like or disk-like. Our analysis leads us to the following conclusions.

1. Stream-like fields have blue RCs and extended horizontal branches yet are more metal enriched than disk-like fields. They show no evidence of recent star formation. Our analysis reveals for the first time that the western shelf (probed by the EC1_field) is consistent with being material torn off from the GS progenitor. We compare the spatial and line-of-sight distribution of stream-like fields with the F07 simulation of the GS progenitor orbit and find an excellent agreement. In this picture, the GS and Brown-stream fields sample the giant stream itself while the NE shelf and EC1_field probe the northeastern and western shelves. The minor axis and Brown-spheroid fields are significantly contaminated by stream material that has undergone several pericentric passages, as previously suspected from kinematics (Gilbert et al. 2007).
2. Disk-like fields have rounder RCs which have significant luminosity width and show no evidence of an extended horizontal branch. All show evidence for young ($\lesssim$2 Gyr) populations, and in some cases star formation as recent as 250 Myr ago. Disk-like material could have either an external or an internal origin. Recent work (e.g., Kazantzidis et al. 2007) describes how such structures resembling tidal debris can be created from interactions between the stellar thin disk and massive satellites on close pericentric orbits. Given the uniform populations in these fields, including the ubiquitous presence of young populations, and the high rotation observed in the extended disk to which the disk-like fields belong (Ibata et al. 2005), we favor this scenario over the original assertion that this vast extended rotating component has formed via accretion.
3. Several fields are identified as being "composite" in the sense of having both stream-like and disk-like properties. Amongst these are the Brown-odisk and Brown-spheroid fields which have been the targets of ultra-deep *HST* programs aimed at determining the SFH of the M31 disk and halo back to the earliest times (Brown et al. 2006a). Our findings indicate that the stellar populations in these regions are probably much more complicated than originally envisioned, making interpretation of the resulting SFHs difficult. Another composite field is the NGC205 loop. We have shown that this field likely contains GS contamination in addition to an underlying component which is consistent with being either material from NGC205 and/or from M31's extended disk.

We have shown that much insight can be gained into the nature and origin of substructure in M31 from the comparative analysis of CMDs reaching a few magnitudes below the RC. As new surveys uncover an ever-increasing level of complexity in this system, a shallow-depth multi-pointing approach such as this may prove very valuable. In forthcoming work, we will

present detailed SFH fits in the various fields analyzed here as a means to confirm and better quantify their similarities and differences. It will also be of great interest to extend this analysis to the tidal streams recently discovered in the far outer halo by Ibata et al. (2007).

We thank David Thilker for providing M31 H I column density values ahead of publication and Mark Fardal for providing us with the data-points to produce Figure 8. We wish to thank Tom Brown for discussions during the early stages of this project and P. Stetson for providing his stand-alone DAOPHOT II code. J.C.R. acknowledges the award of an STFC studentship. A.M.N.F. is supported by a Marie Curie Excellence Grant from the European Commission under contract MCEXT-CT-2005-025869. N.R.T. acknowledges financial support via a STFC Senior Research Fellowship. Support for programs GO9458 and GO10128 was provided by NASA through a grant from the Space Telescope Science Institute, which is operated by the Association of Universities for Research in Astronomy, Inc., under NASA contract NAS5-26555.

REFERENCES

Alves, D. R., & Sarajedini, A. 1999, ApJ, 511, 225
Bellazzini, M., Cacciari, C., Federici, L., Fusi Pecci, F., & Rich, M. 2003, A&A, 405, 867
Belokurov, V., et al. 2007, ApJ, 658, 337
Brinks, E., & Burton, W. B. 1984, A&A, 141, 195
Brown, T. M., Ferguson, H. C., Smith, E., Kimble, R. A., Sweigart, A. V., Renzini, A., Rich, R. M., & VandenBerg, D. A. 2003, ApJ, 592, L17
Brown, T. M., Smith, E., Ferguson, H. C., Rich, R. M., Guhathakurta, P., Renzini, A., Sweigart, A. V., & Kimble, R. A. 2006a, ApJ, 652, 323
Brown, T. M., Smith, E., Guhathakurta, P., Rich, R. M., Ferguson, H. C., Renzini, A., Sweigart, A. V., & Kimble, R. A. 2006b, ApJ, 636, L89
Brown, T. M., et al. 2005, AJ, 130, 1693
Brown, T. M., et al. 2007, ApJ, 658, L95
Bullock, J. S., & Johnston, K. V. 2005, ApJ, 635, 931
Butler, D. J., & Martínez-Delgado, D. 2005, AJ, 129, 2217
Carney, B. W., Latham, D. W., & Laird, J. B. 2005, AJ, 129, 466
Choi, P. I., Guhathakurta, P., & Johnston, K. V. 2002, AJ, 124, 310
Davies, M. B., Piotto, G., & de Angeli, F. 2004, MNRAS, 349, 129
Dolphin, A. E., Weisz, D. R., Skillman, E. D., & Holtzman, J. A. 2005, arXiv astro-ph/0506430
Fardal, M. A., Babul, A., Geehan, J. J., & Guhathakurta, P. 2006, MNRAS, 366, 1012
Fardal, M. A., Guhathakurta, P., Babul, A., & McConnachie, A. W. 2007, MNRAS, 380, 15
Faria, D., Johnson, R. A., Ferguson, A. M. N., Irwin, M. J., Ibata, R. A., Johnston, K. V., Lewis, G. F., & Tanvir, N. R. 2007, AJ, 133, 1275
Ferguson, A. M. N., Irwin, M. J., Ibata, R. A., Lewis, G. F., & Tanvir, N. R. 2002, AJ, 124, 1452
Ferguson, A. M. N., & Johnson, R. A. 2001, ApJ, 559, L13
Ferguson, A. M. N., Johnson, R. A., Faria, D. C., Irwin, M. J., Ibata, R. A., Johnston, K. V., Lewis, G. F., & Tanvir, N. R. 2005, ApJ, 622, L109
Font, A. S., Johnston, K. V., Bullock, J. S., & Robertson, B. E. 2006a, ApJ, 638, 585
Font, A. S., Johnston, K. V., Ferguson, A. M. N., Bullock, J. S., Robertson, B. E., Tumlinson, J., & Guhathakurta, P. 2008, ApJ, 673, 215
Font, A. S., Johnston, K. V., Guhathakurta, P., Majewski, S. R., & Rich, R. M. 2006b, AJ, 131, 1436
Gauthier, J.-R., Dubinski, J., & Widrow, L. M. 2006, ApJ, 653, 1180
Gilbert, K. M., et al. 2007, ApJ, 668, 245
Girardi, L., Bressan, A., Bertelli, G., & Chiosi, C. 2000, A&AS, 141, 371
Girardi, L., & Salaris, M. 2001, MNRAS, 323, 109
Grillmair, C. J., & Dionatos, O. 2006, ApJ, 643, L17
Harris, J., & Zaritsky, D. 2001, ApJS, 136, 25
Helmi, A., & White, S. D. M. 1999, MNRAS, 307, 495
Hodge, P. W. 1973, ApJ, 182, 671
Holland, S., Fahlman, G. G., & Richer, H. B. 1996, AJ, 112, 1035
Ibata, R., Chapman, S., Ferguson, A. M. N., Irwin, M., Lewis, G., & McConnachie, A. 2004, MNRAS, 351, 117
Ibata, R., Chapman, S., Ferguson, A. M. N., Lewis, G., Irwin, M., & Tanvir, N. 2005, ApJ, 634, 287
Ibata, R., Irwin, M., Lewis, G., Ferguson, A. M. N., & Tanvir, N. 2001, Nature, 412, 49
Ibata, R., Martin, N. F., Irwin, M., Chapman, S., Ferguson, A. M. N., Lewis, G. F., & McConnachie, A. W. 2007, ApJ, 671, 1591
Irwin, M. J., Ferguson, A. M. N., Ibata, R. A., Lewis, G. F., & Tanvir, N. R. 2005, ApJ, 628, L105
Johnston, K. V., Hernquist, L., & Bolte, M. 1996, ApJ, 465, 278
Kazantzidis, S., Bullock, J. S., Zentner, A. R., Kravtsov, A. V., & Moustakas, L. A. 2007, arXiv:0708.1949
Koekemoer, A. M., Fruchter, A. S., Hook, R. N., Hack, W., & Hanley, C. 2006, in The 2005 HST Calibration Workshop: Hubble After the Transition to Two-Gyro Mode, ed. A. M. Koekemoer, P. Goudfrooij, & L. L. Dressel, 423
Mackey, A. D., et al. 2006, ApJ, 653, L105
Mackey, A. D., et al. 2007, ApJ, 655, L85
Majewski, S. R., Skrutskie, M. F., Weinberg, M. D., & Ostheimer, J. C. 2003, ApJ, 599, 1082
Martin, N. F., Ibata, R. A., Irwin, M. J., Chapman, S., Lewis, G. F., Ferguson, A. M. N., Tanvir, N., & McConnachie, A. W. 2006, MNRAS, 371, 1983
McConnachie, A. W., Irwin, M. J., Ferguson, A. M. N., Ibata, R. A., Lewis, G. F., & Tanvir, N. 2005, MNRAS, 356, 979
McConnachie, A. W., Irwin, M. J., Ibata, R. A., Ferguson, A. M. N., Lewis, G. F., & Tanvir, N. 2003, MNRAS, 343, 1335
McConnachie, A. W., Irwin, M. J., Lewis, G. F., Ibata, R. A., Chapman, S. C., Ferguson, A. M. N., & Tanvir, N. R. 2004, MNRAS, 351, L94
Mori, M., & Rich, R. M. 2008, ApJ, 674, L77
Mould, J., & Kristian, J. 1986, ApJ, 305, 591
Paczynski, B., & Stanek, K. Z. 1998, ApJ, 494, L219
Peñarrubia, J., McConnachie, A., & Babul, A. 2006, ApJ, 650, L33
Quinn, P. J., Hernquist, L., & Fullagar, D. P. 1993, ApJ, 403, 74
Reitzel, D. B., Guhathakurta, P., & Rich, R. M. 2004, AJ, 127, 2133
Schlegel, D. J., Finkbeiner, D. P., & Davis, M. 1998, ApJ, 500, 525
Sirianni, M., et al. 2005, PASP, 117, 1049
Steinmetz, M., & Navarro, J. F. 2002, New Astron., 7, 155
Stetson, P. B. 1987, PASP, 99, 191
van den Bosch, F. C., Lewis, G. F., Lake, G., & Stadel, J. 1999, ApJ, 515, 50
Velazquez, H., & White, S. D. M. 1999, MNRAS, 304, 254
Walker, I. R., Mihos, J. C., & Hernquist, L. 1996, ApJ, 460, 121
White, S. D. M., & Frenk, C. S. 1991, ApJ, 379, 52
Williams, B. F. 2001, BAAS, 33, 1380
Zucker, D. B., et al. 2004, ApJ, 612, L117